# Brownian dynamics simulation of dense binary colloidal mixtures. I. Structural evolution and dynamics

Subrata Sanyal* and Ajay K. Sood†
*Department of Physics, Indian Institute of Science, Bangalore 560 012, India*
(Received 21 February 1995)

We have carried out Brownian dynamics simulations of binary mixtures of charged colloidal suspensions of two different diameter particles with varying volume fractions $\phi$ and charged impurity concentrations $n_i$. For a given $\phi$, the effective temperature is lowered in many steps by reducing $n_i$ to see how structure and dynamics evolve. The structural quantities studied are the partial and total pair distribution functions $g(r)$, the static structure factors, the time average $g(\bar{r})$, and the Wendt-Abraham parameter. The dynamic quantity is the temporal evolution of the total mean-squared displacement (MSD). All these parameters show that by lowering the effective temperature at $\phi = 0.2$, liquid freezes into a body-centered-cubic crystal whereas at $\phi = 0.3$, a glassy state is formed. The MSD at intermediate times shows significant subdiffusive behavior whose time span increases with a reduction in the effective temperature. The mean-squared displacements for the supercooled liquid with $\phi = 0.3$ show staircase behavior indicating a strongly cooperative jump motion of the particles.

PACS number(s): 82.70.Dd, 61.20.Ja, 05.40.+j, 64.70.Dv

## I. INTRODUCTION

Computer simulations have provided decisive insight into the structural and dynamical aspects of the liquid to crystalline transition (CT) [1,2] as well as the liquid to glass transition (GT) [3,4]. The recent use of the nonlinear mode-coupling theory (MCT) [5] of dense liquids to glass formation has given an impetus to the study of the GT. Detailed comparisons of the experimental and the computer simulation results with the MCT predictions have been performed on diverse systems such as ionic systems, e.g., $Ca_{0.4}K_{0.6}(NO_3)_{1.4}$ [6], and molecular systems e.g., propylene carbonate [7,8], polymers [9], proteins [10], and hard-sphere colloids [11–13].

The ease in controlling the interparticle interactions merely by varying the impurity-ion concentration $n_i$ and the particle volume fraction $\phi$ [14] makes the aqueous suspensions of charged polystyrene spheres (polyballs) ideal model systems for studies concerning crystallization as well as glass formation. The earlier simulations on polyballs were concerned with the study of the order-disorder transition [15–21] and glass formation [21,22]. The molecular dynamics (MD) simulations for the phase diagram of monodisperse Yukawa system [15,16] have shown the existence of liquid, body-centered-cubic (bcc), and face-centered-cubic (fcc) phases, in qualitative agreement with laboratory experiments [23,24]. In the small-angle neutron scattering experiments [24], the glassy state was also shown to exist at high volume fractions ($\phi > 0.2$). The pair distribution functions (PDF's) obtained from the Fourier transform of the measured static structure factors $S(q)$ indicated that the short-range order in the glassy state is fcc-like. In the MD simulations using the Derjaguin-Landau-Verway-Overbeek (DLVO) potential [Eq. (1)], a spontaneous freezing of liquid into a bcc phase was observed at a critical density [17], which is to be contrasted with the result of Robbins *et al.* [15,16], where the spontaneous crystallization was absent except for only two runs. The Monte Carlo simulations of the polyball system has been carried out to study the order-disorder transition without any specific reference to the bcc or the fcc phase [18,19]. The MD simulations for a 1:1 binary mixture of polyballs [20] interacting via the DLVO potential with the parameters similar to the experiments by Lindsay and Chaikin [25] (and also to the present simulations) have shown transitions from a liquid to a crystal and a liquid to a glassy state as $\phi$ is increased. We will comment on this study later. Polydispersity is known to favor the glass forming tendencies of a system by inhibiting crystallization. Colloidal systems can possess both size polydispersity as well as charge polydispersity. About 11% of size polydispersity is shown to disrupt the crystalline order [26–28]. The results of the recent MC simulations by Tata and Arora [21] indicate a charge-polydispersity-driven crystal to a glass transition at a charge polydispersity of about 26% in polyball suspensions.

Since the fluid molecules are much smaller than the polyballs, they provide a viscous damping to the motion of the polyballs. Hence the simulation technique appropriate to the polyball suspensions is Brownian dynamics

*Present address: Department of Chemical and Nuclear Engineering, University of California at Santa Barbara, Santa Barbara, CA 93106. Electronic address: subrata@squid.ucsb.edu

†Also at Jawaharlal Nehru Centre for Advanced Scientific Research, Jakkur Campus, P.O. Jakkur, Bangalore 560 064, India. Electronic address: asood@physics.iisc.ernet.in

 

(BD), which was proposed by Ermak *et al.* [29,30] and has been used in earlier simulations [31]. The influence of the Newtonian MD *vis-à-vis* the Brownian dynamics on the dynamical correlations for the liquid to GT in charge-polydisperse colloids has been investigated in a previous simulation study [22]. It was shown that the long-time relaxation behaviors of the density correlation functions in both cases are similar even though they differ in short and intermediate times.

In this paper we report the results of our BD simulations of a binary system of polyballs with different radii and charges. The aim has been to study how the structure evolves as the interaction between the polyballs is increased either by increasing the volume fraction $\phi$ or by reducing the charged ion concentration $n_i$. This is equivalent to reducing the effective temperature of the fluid towards freezing into a crystalline state or towards supercooling to a metastable glassy state. We find that for $\phi = 0.2$, the liquid to crystal transition takes place at an effective temperature $T_f^\star = 0.0374$, but for $\phi = 0.3$, the liquid goes into a glassy state at $T_g^\star \simeq 0.0312$. In the following paper (hereafter called paper II) [32], we present the study of the translational and bond-orientational order of these states, while the evolution of the van Hove correlation functions is reported elsewhere [33]. The rest of the paper is set up as follows. In Sec. II we describe the model and the details of the simulation. Section III is devoted to the results of our simulation. Finally, Sec. IV contains the summary of our findings and conclusions of this work.

## II. MODEL AND DETAILS OF SIMULATION

We consider an equimolar [i.e., the composition variable $x = N_1/(N_1+N_2) = 0.5$] binary mixture of charged spherical polyballs of $N_1$ and $N_2$ particles with radii $a_1$ and $a_2$ ($> a_1$), respectively. The interaction between all the pairs $(i,j)$ of particles separated by a center-to-center distance $r = |\vec{r}_i - \vec{r}_j|$ is modeled via the purely repulsive size-corrected DLVO potential [14]

$$U_{ij}(r) = \frac{Z_i Z_j e^2}{\epsilon}\left(\frac{e^{\kappa a_i}}{1+\kappa a_i}\right)\left(\frac{e^{\kappa a_j}}{1+\kappa a_j}\right)\frac{e^{-\kappa r}}{r}, \qquad (1)$$

where $a_s = n_p^{-1/3}$ is the average interparticle separation, $Z_i$ is the effective valence on species $i$, and $\epsilon$ is the dielectric constant of water (equal to 78) at temperature $T$ (equal to 298 K). The inclusion of the geometrical factor $\exp[\kappa(a_i+a_j)]/(1+\kappa a_i)(1+\kappa a_j)$ is like incorporating the hard-core repulsion [14,17]. For a binary suspension, the inverse Debye-Hückel screening length $\kappa$ is given by

$$\kappa^2 = \frac{4\pi e^2}{\epsilon k_B T}\left(n_p \bar{Z} + \sum_i n_i z_i^2\right), \qquad (2)$$

where $n_p$ and $n_i$ are the total number densities of the particles and the monovalent impurity ions (i.e., $z_i = 1$), respectively. Here $\bar{Z} = xZ_1 + (1-x)Z_2$ and $k_B$ is the Boltzmann constant.

The cutoff distance $r_c$ for the potential is chosen to be equal to $2a_s$ or $6\kappa^{-1}$, whichever is greater, to ensure that $U_{ij}(r_c) \sim 0.001 k_B T$. The bulk of our simulations were carried out with $N\ (= N_1 + N_2) = 432$ particles confined to a cubic box (of volume $V$), whose dimensions are adjusted to get the appropriate number density $n_p = N/V$. We have used the cubic periodic boundary conditions and its natural consequence—the minimum image convention [34]—to minimize the surface effects. The system can be suitably characterized by its total volume fraction

$$\phi = \frac{4}{3}\pi n_p [x a_1^3 + (1-x)a_2^3] \qquad (3)$$

and reduced temperature $T^\star$, given by

$$\frac{1}{T^\star} = \frac{U_0}{k_B T} = \frac{(\bar{Z}e)^2}{\epsilon k_B T}\left(\frac{e^{\kappa \bar{a}}}{1+\kappa \bar{a}}\right)^2 \frac{e^{-\kappa a_s}}{a_s}, \qquad (4)$$

where $\bar{a}$ is the mean radius and $U_0$ is the energy scale. Our system is identical to the experimental system of Lindsay and Chaikin [25] as well as the one used in the MD simulation of Rosenberg *et al.* [20], viz., $a_1 = 545$ Å, $a_2 = 1100$ Å, $Z_1 = 300$, $Z_2 = 600$, and $x = 0.5$.

Following Ermak and Yeh [29], we use the finite difference BD algorithm in which the hydrodynamic interactions are neglected and the stochastic Langevin equations of motion are integrated in a finite time interval $\delta t$ to update the particle positions $\{\vec{r}_i(t)\}$:

$$\vec{r}_i(t+\delta t) = \vec{r}_i(t) + \frac{D_0}{k_B T}\vec{F}_i(t)\delta t + (\Delta \vec{r})_R + O((\delta t)^2). \qquad (5)$$

The random displacements $(\Delta \vec{r})_R$ are sampled from a Gaussian distribution with zero mean and variance $\langle (\Delta \vec{r})_R^2 \rangle = 6 D_0 \delta t$. We note that the variance is directly proportional to the absolute temperature $T$ through the Stokes-Einstein relation $D_0 = k_B T/\xi = k_B T/(6\pi\eta a_p)$, where $\xi$ is the macroscopic friction coefficient, $\eta$ is the viscosity of solvent (equal to 0.010 89 P for water), and $a_p$ is the hydrodynamic radius of the particle. Since the primary objective of the present work is to investigate the long-time behavior of the dynamical correlation functions [32] near the liquid to solid (crystal or glass) transition, the choice of $\delta t$ should be such that the long-time behavior is reached in an optimum number of time steps. On the other hand, since the error associated with the BD algorithm [Eq. (5)] is $O((\delta t)^2)$, a reasonable stability of the trajectory is ensured provided the integration time step $\delta t$ is chosen to be much smaller than the density relaxation time $\tau_d$ ($\simeq a_s^2/D_0 \sim 10^{-3}$ sec) but much larger than the velocity relaxation time $\tau_v = \frac{M}{\xi}$ ($\sim 10^{-8}$ sec), where $M$ is the particle mass. The value $\delta t \simeq 10^{-6}$ sec was found to be a satisfactory choice to ensure a reasonable stability of the trajectories for the highest values of $\phi$ and $\kappa^{-1}$ studied. Due to the above choice of $\delta t \gg \tau_v$, the dynamics is coarse grained, rendering the momentum variables $\vec{p}_j$ absent in the BD.

Due to the inaccuracies in calculating the systematic part [i.e., the second term on the right-hand side of Eq.

(5)] and the random part $(\Delta\vec{r})_R$ of Eq. (5), there could be a small shift of the center of mass of the total system, resulting in a spurious, monotonic increment of the mean-squared displacement (MSD). This contribution, though very small, will not allow the MSD to saturate to a finite value when the underlying order of the system is solid-like. This is corrected by holding the center of mass of the system fixed at each position updating.

As a check on the algorithm, we have carried out the center of mass corrected BD simulation for a monodisperse polyball system ($N = 500$, radius $a_p = 455$ Å, valence $Z_p = 450$, $\phi = 0.04$). The fcc phase was found to melt when $n_i = (41 \pm 0.5)$ $\mu$M of HCl, i.e., $n_i = (4.94 \pm 0.06) \times 10^{16}$ cm$^{-3}$. This can be compared with the MD simulations [35] result of $n_i = (31 \pm 1)$ $\mu$M of HCl and the experimental [25] value of $n_i \sim 50$ $\mu$M of HCl.

As shown in Table I, at each $\phi$, an initial bcc lattice is melted into liquid with high impurity concentration $n_i = 5n_p\bar{Z}$ and this liquid is then sequentially "cooled" in 11 more steps with $n_i$ at every step being half of the previous one, except for the last step, where $n_i = 0$. The runs in the sequence are named as L0, La, Lc, ..., Lk for $\phi = 0.01$, X0, Xa, Xc, ..., Xk for $\phi = 0.2$, and G0, Ga, Gc, ..., Gk for $\phi = 0.3$. With this method of cooling, called "slow quench" (SQ), the effective temperature of the system is brought down from $T^\star \sim 1$ to $T^\star \sim 0.03$. To ensure proper equilibration of the system at each $T^\star$,

TABLE I. Cooling history of different runs. The parameters are explained in the text.

| Run | $N_{eq}$ | $N_{pr}$ | $n_i/(n_p\bar{Z})$ | $T^\star$ | $\kappa a_s$ | $E$ | Initial | Final |
|---|---|---|---|---|---|---|---|---|
| | | | $\phi = 0.01$, time step $\delta t = 3.5 \times 10^{-5}$ sec | | | | | |
| L0 | 60000 | | 5 | 1.3045 | 5.995 | 3.64 | bcc | liquid |
| La | 60000 | | 5/2 | 0.3618 | 4.579 | 11.46 | L0 | liquid |
| Lb | 60000 | | 5/4 | 0.1571 | 3.671 | 27.27 | La | liquid |
| Lc | 60000 | | 5/8 | 0.0941 | 3.120 | 48.26 | Lb | liquid |
| Ld | 60000 | | 5/16 | 0.0700 | 2.804 | 69.58 | Lc | liquid |
| Le | 60000 | | 5/32 | 0.0596 | 2.632 | 86.12 | Ld | liquid |
| Lf | 60000 | | 5/64 | 0.0547 | 2.541 | 96.58 | Le | liquid |
| Lg | 60000 | | 5/128 | 0.0523 | 2.495 | 102.45 | Lf | liquid |
| Lh | 120000 | | 5/256 | 0.0512 | 2.471 | 105.36 | Lg | liquid |
| Li | 60000 | | 5/512 | 0.0506 | 2.459 | 106.82 | Lh | liquid |
| Lj | 60000 | | 5/1024 | 0.0503 | 2.453 | 107.59 | Li | liquid |
| Lk | 134950 | 109000 | 0 | 0.0501 | 2.447 | 108.48 | Lj | liquid |
| | | | $\phi = 0.2$, time step $\delta t = 7 \times 10^{-6}$ sec | | | | | |
| X0 | 200000 | 199000 | 5 | 0.9098 | 9.877 | 5.28 | bcc | liquid |
| Xa | 200000 | 199000 | 5/2 | 0.2749 | 7.544 | 14.30 | X0 | Liquid |
| Xb | 200000 | 199000 | 5/4 | 0.1216 | 6.048 | 31.82 | Xa | liquid |
| Xc | 249000 | 199000 | 5/8 | 0.0722 | 5.140 | 55.88 | Xb | liquid |
| Xd | 200000 | 199000 | 5/16 | 0.0530 | 4.620 | 77.71 | Xc | liquid |
| Xe | 200000 | 199000 | 5/32 | 0.0446 | 4.336 | 94.49 | Xd | liquid |
| Xf | 200000 | 199000 | 5/64 | 0.0407 | 4.187 | 104.96 | Xe | liquid |
| Xg | 200000 | 199000 | 5/124 | 0.0388 | 4.110 | 110.89 | Xf | liquid |
| Xh | 200000 | 199000 | 5/256 | 0.0378 | 4.071 | 114.18 | Xg | liquid |
| Xi | 200000 | 199000 | 5/512 | 0.0374 | 4.052 | 119.67 | Xh | bcc |
| Xj | 200000 | 199000 | 5/1024 | 0.0372 | 4.042 | 117.85 | Xi | bcc |
| Xk | 219300 | 199000 | 0 | 0.0369 | 4.032 | 118.67 | Xj | bcc |
| Xl | 200000 | 199000 | 0 | 0.0369 | 4.032 | 118.45 | bcc | bcc |
| Xm | 200000 | 199000 | 0 | 0.0369 | 4.032 | 110.74 | bcc | bcc |
| | | | $\phi = 0.3$, time step $\delta t = 3 \times 10^{-6}$ sec | | | | | |
| G0 | 350000 | 399000 | 5 | 0.5055 | 10.570 | 8.56 | bcc | liquid |
| Ga | 399000 | 399000 | 5/2 | 0.1796 | 8.073 | 21.37 | G0 | liquid |
| Gb | 350000 | 399000 | 5/4 | 0.0876 | 6.472 | 44.22 | Ga | liquid |
| Gc | 350000 | 399000 | 5/8 | 0.0550 | 5.500 | 73.20 | Gb | liquid |
| Gd | 350000 | 399000 | 5/16 | 0.0416 | 4.943 | 100.66 | Gc | liquid |
| Ge | 437230 | 399000 | 5/32 | 0.0356 | 4.639 | 119.18 | Gd | liquid |
| Gf | 350000 | 399000 | 5/64 | 0.0327 | 4.480 | 131.25 | Ge | liquid |
| Gg | 350000 | 399000 | 5/128 | 0.0313 | 4.398 | 137.92 | Gf | glass |
| Gh | 542150 | 399000 | 5/256 | 0.0307 | 4.356 | 141.41 | Gg | glass |
| Gi | 350000 | 399000 | 5/512 | 0.0303 | 4.335 | 143.14 | Gh | glass |
| Gj | 350000 | 399000 | 5/1024 | 0.0302 | 4.325 | 144.12 | Gi | glass |
| Gk | 359600 | 399000 | 0 | 0.0300 | 4.314 | 145.12 | Gj | glass |

the internal energy per particle $E$, together with the total and the partial static pair distribution functions (PDF's), is monitored over the whole equilibration run of $N_{\rm eq}$ time steps ($\sim 10^6 \delta t$). The quantity $E$ (in units of thermal energy $k_B T$) is defined as

$$E = \frac{U_N}{N k_B T} = \frac{1}{N k_B T} \sum_{j \neq i} U_{ij}(r), \tag{6}$$

where $U_{ij}(r)$ is given by Eq. (1). The stability of the trajectories is ensured by the steady value of $E$ (the rms deviation being less than or equal to 0.15%). The next $N_{\rm pr}$ (approximately equal to $N_{\rm eq}$) steps (production run) (see Table I) are used for evaluating the static properties, the MSD's, and the translation and bond-orientational correlation functions (presented in paper II [32]). Thermodynamic quantities are averaged over a few hundred $\delta t$ for fluidlike order and over a few thousand $\delta t$ for solidlike order to keep the error bars less than 5%. That the system has indeed reached an equilibrium state after $N_{\rm eq}$ steps is also ensured from a complete overlap of the total and the partial PDF's calculated at the end of the equilibration (after $N_{\rm eq}$ steps) and production runs (after $N_{\rm eq} + N_{\rm pr}$ steps).

## III. RESULTS

In this section, we report the results of our BD simulation study of the static structural parameters and the total mean-square displacement as a binary dense liquid is cooled by reducing $n_i$ in 12 steps for $\phi = 0.01$, 0.2, and 0.3. By comparing the respective pair distribution functions and mean-squared displacements, we have confirmed that the final state of this cooling process ($n_i = 0$) is a liquid for $\phi = 0.01$, a crystal for $\phi = 0.2$, and a glass for $\phi = 0.3$. The dependence of the results on the system size as well as on the methods of cooling is discussed in Sec. III A. In Sec. III B we study the structural parameters and Sec. III C deals with the total MSD.

### A. Cooling diagram, dependence on system size, and cooling methods

Figure 1 summarizes the cooling diagram in the $\phi$ versus $n_i$ parameter space as obtained from our slow-quench simulations. The characteristics of the corresponding BD runs, namely, the equilibration time steps $N_{\rm eq}$, the production time steps $N_{\rm pr}$, the added salt concentration $n_i/(n_p \bar{Z})$, the temperature $T^\star$, the screening length $\kappa a_s$, and the internal energy per particle $E$, are listed in Table I. The starting configuration and the final state are also given for each run in Table I. The state of a system is characterized by the corresponding PDF and the MSD. A constant $T^\star$ (= 0.04) line in Fig. 1 serves as an approximate freezing boundary. As mentioned earlier, we will concentrate on only three volume fractions ($\phi$), namely, 0.01, 0.2, and 0.3, with different $n_i$. The existence of a crystalline phase in this diagram, in between a liquid region for low $\phi$ and a metastable glass

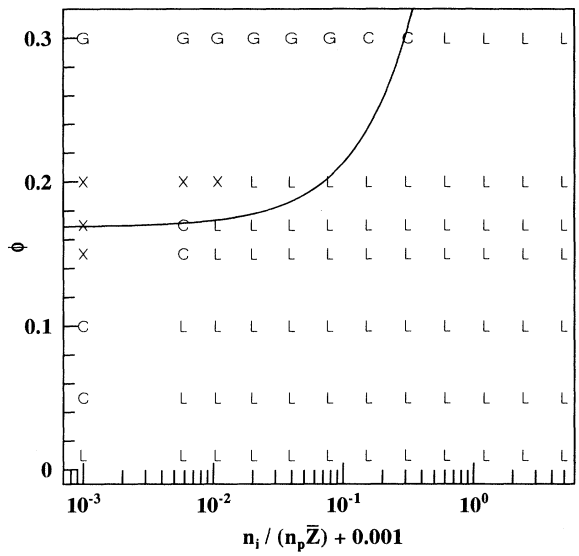


FIG. 1. "Cooling" diagram in the $\phi$ vs $n_i$ parameter space obtained via the slow-quench method. The abbrevations are L, liquid; X, compositionally disordered bcc crystal; G, glass; and C, solid-liquid coexistence. All these states are confirmed from the nature of their PDF and MSD. The solid line corresponds to an approximate freezing boundary of constant $T^\star$ (= 0.04). The $n_i$ axis is shifted and shown in logarithmic scale for convenience.

for higher $\phi$, is in qualitative agreement with our diffusing wave spectroscopy (DWS) experiments on a binary polyball system [36].

As can be noted from Table I, runs Xl and Xm are independent runs and are not similar to the other SQ runs. If the particles are put on bcc lattice positions irrespective of their types and then simulated with the same parameters as run Xk (i.e., $\phi = 0.2$ and $n_i = 0$), the final state Xl is a bcc with improper sublattice ordering. By contrast, if an initial bcc lattice composed of two interpenetrating simple cubic (sc) sublattices made of either kind of particle is simulated with the same parameters as above, the final state Xm is a substitutionally ordered bcc lattice. By comparing the internal energy $E$ and the PDF in subsection III B 4, the position and type of the immediate eight neighbors of each particle and translational and bond-orientational orders in paper II [32], of runs Xk, Xl, and Xm, we conclude [37] that the resulting final state Xk of our slow-quench simulation is a compositionally disordered bcc lattice, similar to Xl. We believe that this is a limitation due to the finite size and the finite time of our simulation and probably also due to a high energy barrier; otherwise the system would have reached its proper equilibrium state given by run Xm.

We consider three different cooling methods: (i) the slow quench (SQ), (ii) the rapid quench (RQ), and (iii) the density quench (DQ). In the first two methods, the system at a constant $\phi$ is effectively cooled by reduc-

ing $n_i$. An initial lattice [bcc ($N = 250$ or 432) or fcc ($N = 256$ or 500 or 1372) or sodium-chloride structure (NaCl, $N = 512$)] is melted by taking a very high impurity concentration [$n_i/(n_p\bar{Z}) = 5$] to obtain a fluid configuration. In the slow-quench method, this fluid is cooled in 12 steps as stated in Sec. II. In the rapid-quench method, it is cooled to the required value of $n_i$ in one BD step. At every $n_i$ (or $T^*$), the system goes through proper equilibration and production runs. In the density-quench method, $n_i = 0$ and a low-$\phi$ liquid is effectively cooled by increasing $\phi$. Comparisons among the results of these methods are given in the following.

#### 1. Slow-quench versus rapid-quench methods

In the following (also refer to Table II), we compare the final states obtained by cooling a liquid by these two methods. The total number of particles $N$ vary from 250 to 1372.

(a) Far away from the melting-freezing line in the cooling diagram (Fig. 1), these two methods are consistent with each other irrespective of the system size ($N$). To this effect, we find that (refer to Table I) the final $n_i = 0$ state for $\phi = 0.01$ is a liquid by either of these two methods. Similarly, glassy states are obtained for $\phi = 0.3$ by either of these two methods.

(b) Crystallization is extremely sensitive to the cooling procedure and the starting configuration chosen. For $\phi = 0.2$, the RQ method yields a dense liquid or glass for $N = 432$, 500 or 1372. By contrast, via SQ method, a liquid ($\phi = 0.2$, $N = 432$) freezes into a bcc crystal with the lattice positions randomly occupied by either of the particles. The PDF's of the final bcc states obtained by the RQ method for $N = 256$ and $\phi = 0.15$, 0.18, or 0.21 show compositional disorder similar to the SQ results for $N = 432$. In the former case, quite surprisingly, the MSD's have always shown a linear dependence on time. We note that unlike $N = 432$, $N = 256$ is not compatible with the bcc structure but rather is compatible with the fcc structure. We believe that even though an overall bcc-like short-range order is favored in the system, the number incompatibility did not allow the $N = 256$ particles' system to freeze into a bcc structure, thereby showing liquidlike behavior in the MSD. The number incompatibility could as well be the reason for the absence of crystallization in the final state of $\phi = 0.2$ system obtained either by SQ ($N = 500$) or by RQ ($N = 500$ or 1372). The latter two numbers are compatible with the fcc structure.

TABLE II. Comparison between the slow-quench (SQ) and the rapid-quench (RQ) methods of cooling. The initial liquid is obtained by melting a lattice, which is given in parentheses in the column specifying the system size $N$. The final state, as confirmed from the PDF's and MSD's, is also provided: L, liquid; DL, dense liquid; G, glass; Sat., saturating; Gr., growing; and Int., intermediate.

| | | | Final state | |
|---|---|---|---|---|
| $\phi$ | Method | $N$ (Lattice) | PDF's | MSD's |
| 0.01 | SQ | 250 (bcc)<br>256 (fcc) | L | Gr. |
| | RQ | 432 (bcc)<br>500 (fcc) | | |
| 0.15 or 0.18 or 0.21 | SQ | 432 (bcc) | bcc | Sat. |
| | RQ | 256 (fcc) | bcc | Gr. |
| 0.2 | RQ | 432 (bcc)<br>500 (fcc)<br>1372 (fcc) | DL-G | Int. |
| 0.3 | SQ | 432 (bcc) | bcc | Sat. |
| | | 500 (fcc) | DL-G | Int. |
| | RQ | 256 (fcc)<br>432 (bcc)<br>500 (fcc)<br>512 (NaCl) | G | Sat. |
| | SQ | 432 (bcc) | G | Sat. |

#### 2. Finite-size and finite-time effect on freezing

It is known that the problems associated with the finite size and the finite time of the simulations can become important close to the fluid-solid transition. With the lowest system size $N = 256$, the freezing line (refer to Fig. 1) is found to shift towards lower $\phi$ ($\phi_c \sim 0.0575$) and often towards higher values of $n_i$ than that obtained with larger systems (for example, $\phi_c \sim 0.1$ for $N = 432$). We believe that any amorphous state is metastable and, given enough time, will reach its proper equilibrium state, which is crystalline. To verify this, we use the same parameters corresponding to the glassy states, obtained by the SQ or the RQ methods, to a system of particles put in an initial lattice and run it for a large number of BD steps to find that the final state remains crystalline with the internal energy $E$ lower than that in the glass by about 10%. Even our longest simulation of approximately 10 sec ($\simeq 10^7 \delta t$!) was not enough for a glass ($\phi = 0.3, n_i = 0$) to reach the lower-energy bcc crystal.

#### 3. Density-quench method: MD versus BD

MD simulations following the DQ method have been carried out by Rosenberg *et al.* [17,20]. In Ref. [20] which deals with a system identical to the present one, it is found that an initial bcc lattice ($N = 1024$) melted into a liquid at $\phi = 0.005$ remains liquid when the density is increased to $\phi = 0.0075$. The mixture spontaneously freezes into a bcc lattice of two interpenetrating sc structures on a subsequent increment of the density to $\phi = 0.01$ and into the glassy states for $\phi > 0.01$. The

glass, upon contraction to $\phi = 0.01$, retrieves the substitutional bcc order. This never happened in our BD simulations for $N = 432$ or 1024. Rather, liquid phase is obtained until $\phi = 0.0575$ and beyond this, it shows a glassy state for higher values of $\phi$, similar to the rapid-quench method. The MD results [20] have also shown that upon equilibration, an initial bcc lattice, with the upper and the lower half of the simulation box containing the smaller and the larger particles, respectively (phase-separated crystal), freezes into a substitutional bcc lattice at $\phi = 0.1$. By contrast, our BD results show that an initial bcc lattice (substitutional or phase separated) melts for $\phi \leq 0.01$, but remains similar to the bcc lattice with increasing rigidity for higher values of $\phi$. The rigidity is inferred from the increased peak heights of $g(r)$ and the reduction in the short-time fluctuations in MSD's.

By comparing the PDF for $\phi = 0.01$, 0.2, and 0.3 with $N = 432$ (slow quench) and 1024 (rapid quench), we found that they completely overlap with each other. From this and the above results, we conclude that in order to simulate proper equilibrium polyball suspensions via the center of mass corrected BD algorithm, the optimum choice of the system size is $N = 432$. Further, the slow-quench method, being the closest approximation of the process of reduction of $n_i$ by the ion-exchange resins in the laboratory experiments, is obviously a better candidate than the density-quench method involving $\phi$ variation at constant $n_i$.

### B. Microscopic structure

The structural parameters that we have probed are the total and the partial PDF, i.e., $g(r)$ and $g_{\alpha\beta}(r)$ ($\alpha, \beta =$ 1 or 2); their respective spatial Fourier transforms, the total and the partial structure factors $S(q)$ and $S_{\alpha\beta}(q)$; the integrated numbers of neighbors, defined as

$$n(r) = 4\pi \int_0^r g(r') r'^2 dr'; \tag{7}$$

and finally an empirical structural parameter, called the Wendt-Abraham parameter $R_g = g_{\min}/g_{\max}$, where $g_{\max}$ and $g_{\min}$ are the values of $g(r)$ at its first maximum and the following first minimum, respectively [38–40].

In order to clearly resolve the structural features that are smeared out by the thermal broadening of the PDF peaks, one can determine the PDF $g(\bar{r})$ defined by the time-averaged positions [41]

$$\bar{r} = |\langle \vec{r}(t) \rangle| = \frac{1}{p+1} \sum_{t'=\frac{t-p}{2\delta t}}^{\frac{t+p}{2\delta t}} \vec{r}(t'). \tag{8}$$

The most appropriate value of the number of steps $p$ for position averaging was found from the minimum in the $R_g$ versus $p$ plots [41]. This corresponds to the typical time for vibration of a particle in a "cage" formed by its immediate neighbors. The values of $p$ obtained by this method are about 200 for liquid (run Lk), 400 for crystal (run Xk), and 100 for glass (run Gk).

#### *1. Liquid, crystalline, and glassy states*

Figure 2 shows $g(r)$ and $g_{\alpha\beta}(r)$ ($\alpha, \beta = 1$ or 2) at $n_i = 0$ for $\phi = 0.01$, 0.2, and 0.3, which have features typical for liquid, crystal, and glassy phases, respectively. The total MSD presented in a later subsection, together with these PDF's confirms the state of the system. The characteristic features of the PDF's in Figs. 2(a) and 2(d) are a broad first peak, a smooth second peak, and a third peak with an appreciably diminished intensity, confirming a complete absence of the long-range order and corresponding to a liquid state. As a further confirmation, only the first peak of $g(\bar{r})$ [or $g_{\alpha\beta}(\bar{r})$] for liquids (not shown in the figure) becomes relatively higher and sharper compared to that in the $g(r)$ [or $g_{\alpha\beta}(r)$].

Figures 2(b) and 2(e) show the PDF's that have pronounced peaks at positions corresponding to a bcc crystal. This is brought out more clearly in the time average $g(\bar{r})$, shown in Fig. 3(a), where the vertical bars indicate the positions of the neighbors in the bcc structure, scaled with respect to the first peak position of $g(r)$. Figures 3(a) (run Xk) and 4 (run Gk) correspond to Figs. 2(b) and 2(c), respectively, showing that the peak structures are far better revealed in $g(\bar{r})$. The vertical bars in the Figs. 4(a) and 4(b) are fcc neighbor positions scaled with respect to the position of the respective primary maximum.

A considerably sharper and narrower first peak compared to the liquidlike states, a split in the second peak, and the presence of a distinct third peak are the characteristic features of a glassy state for $\phi = 0.3$ in Figs. 2(c), 2(f), and 4. A comparison of the PDF for the run Gk (Fig. 4) with run Xk [Fig. 3(a)] confirms a complete absence of nucleation in the former. Very interestingly, we find that $g_{11}(\bar{r})$ [Fig. 4(a)] and $g_{12}(\bar{r})$ (not shown) reveal peak structures commensurate with fcc shell positions for at least a few neighbors, including the presence of a kink at the first-neighbor position and evolution of small peaks at the next three neighbors from the split second peak. By contrast, $g_{22}(\bar{r})$ [Fig. 4(b)] and $g(\bar{r})$ (not shown) show the split second peak at the second and third fcc shell positions. This is similar to the constant pressure Monte Carlo simulations of Lennard-Jones glass [38] wherein a comparison with the experimental results [42] has also been made.

If any of our systems had phase separated, $g_{11}(r)$ and $g_{22}(r)$ should have been significantly higher than $g_{12}(r)$, signaling a tendency towards homocoordination. Lacking such evidence [Figs. 2(a)–2(c)], we rule out the possibility of phase separation in any of our simulations. An interesting feature to be noted in Figs. 2(b) and 2(e) is that the partial PDF's are identical to the total one beyond the first minimum following the first peak. Also, the first peak is shifted to either side of the total one, in conformity with the different hard-sphere radii of the two types of particles. These show that the particles are distributed at random, irrespective of their type, in the final state Xk. In contrast to the crystalline case, the second and the third peaks in the $g_{\alpha\beta}(r)$ of glass with $\phi = 0.3$ [Figs. 2(c) and 2(f)] are shifted to either side of

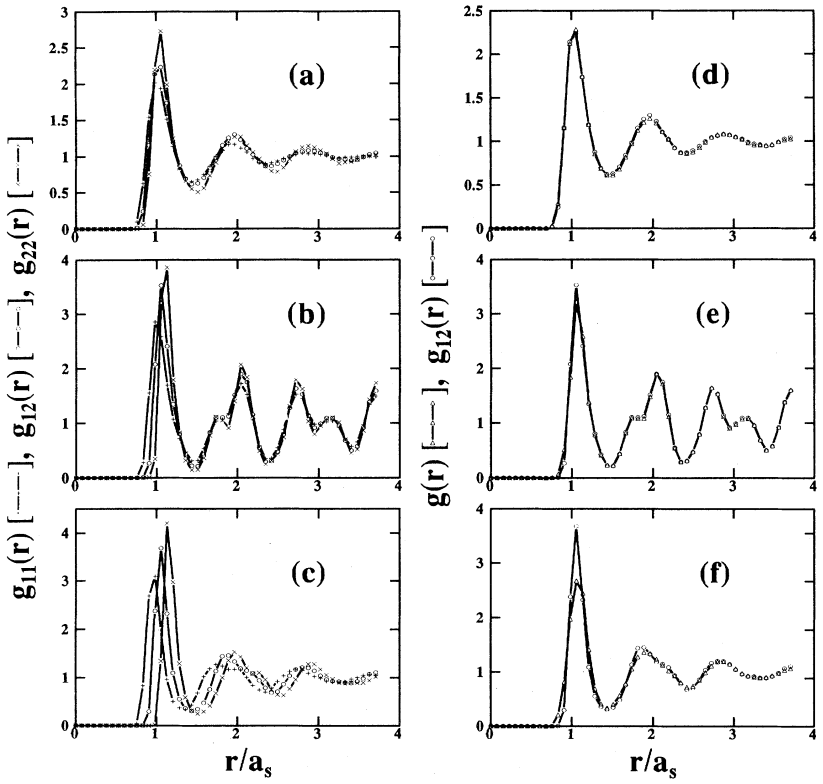


FIG. 2. Partial PDF $g_{\alpha\beta}(r)$ ($\alpha, \beta = 1$ or 2) vs $r/a_s$ for the final $n_i = 0$ state of (a) the liquid ($\phi = 0.01$), (b) the crystal ($\phi = 0.2$), and (c) the glass ($\phi = 0.3$). The respective $g_{12}(r)$ and $g(r)$ are compared in (d)–(f).

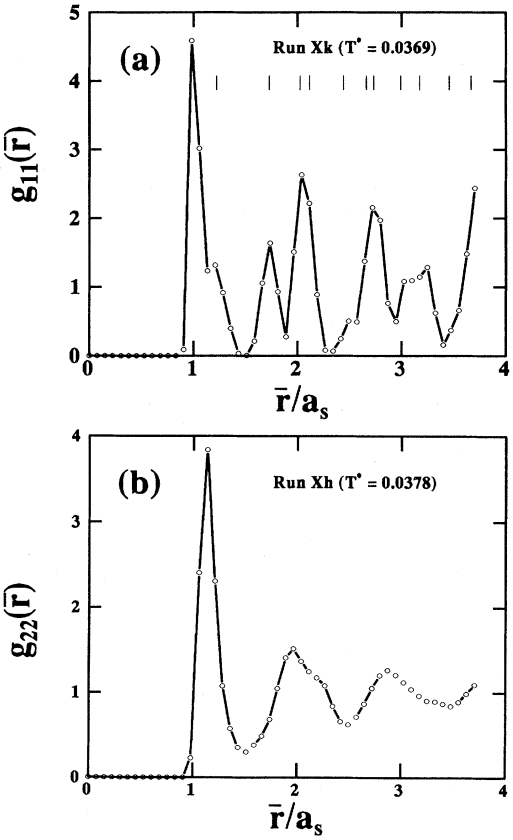


FIG. 3. $g_{11}(\bar{r})$ and $g_{22}(\bar{r})$ defined by the time average of the position vectors $\bar{r}$ for (a) run Xk (bcc crystal) and (b) run Xh, respectively. The small vertical lines in (a) indicate the positions of neighbors in the bcc structure.

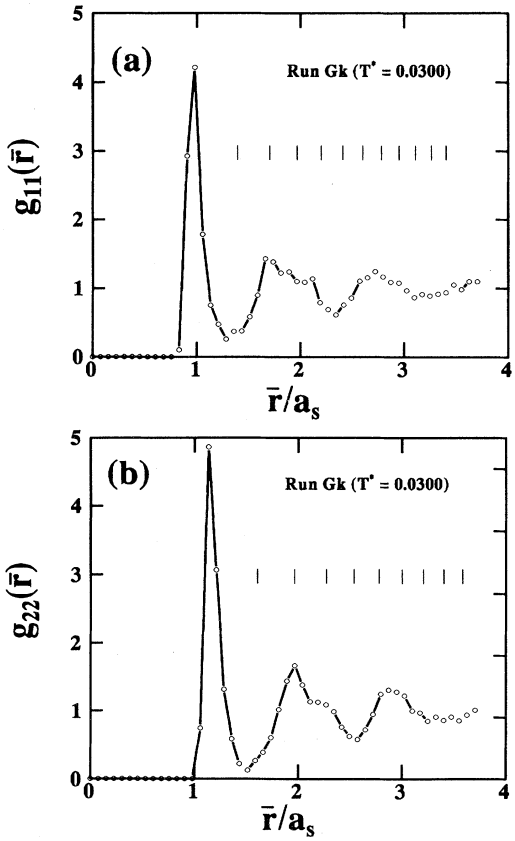


FIG. 4. Partial pair distribution functions, defined by $\bar{r}$, in the run Gk for (a) the lighter and (b) the heavier particles. The small vertical lines in each panel indicate the positions of neighbors in the fcc structure.

the corresponding peaks in $g(r)$ commensurate with the first-peak shift. A similar nature, though not so clear, exists for the liquid with $\phi = 0.01$ [Figs. 2(a) and 2(d)]. Figures 2(d)–2(f) further show that the nature of the total $g(r)$ closely follows $g_{12}(r)$ for all the $\phi$'s, as expected for an equimolar mixture. We also note that there is a tendency towards complete separation between the first and second shells in the equilibrated states ($n_i = 0$) for dense systems (i.e., for $\phi = 0.2$ and 0.3), as reflected by the small values (approximately 0.2) of $g_{\min}$.

Similar characteristic features also exist in $S(q)$ [37] obtained from the spatial Fourier transform of the corresponding $g(r)$. These are not presented here since they do not carry any new information. For $qa_s \leq 50$, $S(q)$ does not show any "interference" effect, in contrast to the MD results of Bernu *et al.* [43], where they find that with increasing $q$, the oscillations in $S(q)$ near $qa_s \sim 10$ go through a minimum followed by a maximum before getting completely dampened.

We note that the splitting of the second peak of $S(q)$ and the PDF are taken to be the "signature" of the GT in experiments [14,42,44] and simulations [41,45]. The origin of splitting in the PDF and the corresponding static structure factors differ [46]. Such splits are always present in the PDF of our system at low temperatures for $\phi = 0.3$ and also in the dense supercooled liquid before the crystallization takes place for $\phi = 0.2$ [Fig. 3(b)]. At these temperatures, the corresponding MSD's tend to saturate and the density and bond-orientational correlation functions show a slow decay (long-time tail). At first sight, we are surprised by the presence of such a splitting in $g_{22}(r)$ even at higher $T^\star$ for $\phi = 0.2$ and 0.3, despite the corresponding MSD's indicating sufficient movements for the heavier particles (type 2) and the corresponding correlation functions showing liquidlike decays in our total simulation duration. This result is in agreement with the earlier MD studies of binary alloys, with either a purely repulsive $r^{-12}$ potential [43] or Lennard-Jones (LJ) interactions [47]. In these studies too the split second peak in the PDF is found to occur well before the GT is reached. Hence the splitting in the second peak alone should not be used as a signature of the glass transition. It has been suggested [44,48] that the split in the second peak is due to a dense random packing and can occur not only in glasses but also in dense supercooled liquids. In a recent work, Clarke and Jónsson [49] have studied this splitting more carefully by decomposing the PDF of monodisperse and binary spherical hard-sphere packings into components according to the local environment of the pairs. It was shown that the second subpeak is due to the linear trimers of spheres whereas the first subpeak has roughly equal contributions from two types of closely related pairs: the face sharing tetrahedra and triangles with adjacent sides (see Ref. [49] for details). In all these cases referred to above [14,41–45,47,48] the first subpeak of the split second peak is higher than the second subpeak, while in the case of random hard-sphere packing, a reversal of the relative intensities of the two subpeaks occurs with increasing interaction (by densification) [50,49]. A similar picture is seen in our simulations for $\phi = 0.2$. The intensities of the subpeaks in $g_{22}(r)$ (run Xh) shown in Fig. 3(b) reverse to show characteristic bcc-like order in the system as soon as it crystalizes with a further increase in interaction in the run Xi [see Fig. 3(a) for run Xk]. By the method of common-neighbor analysis [49], it was indicated that the reversal of the relative subpeak heights in the second peak results from a broadening of the distribution of distances within the linear trimers, while the distribution sharpens for the sharing tetrahedra and adjacent triangles.

### 2. *Evolution of structure*

We shall now discuss the structural changes for $\phi = 0.01$, 0.2, and 0.3 as a function of slow cooling. In panel (a) of Figs. 5–7 we show our results for the PDF at several values of $T^\star$. The $n(r)$ [calculated using Eq. (7)] are given in panel (b) for a smaller range of $r$ containing only the nearest-neighbor shells. The corresponding $S(q)$ are also studied [37], but are not presented here owing to the same reason stated before. Figure 8 shows the evolution of the interparticle interaction as measured by the first peak height $S_{\max}$ of $S(q)$, as a function of $1/T^\star$ for the three volume fractions.

For $\phi = 0.01$ and $n_i = 0$ [Fig. 5(a)], the equilibrium phase is liquid. For all the $n(r)$ in Fig. 5(b), the inflection

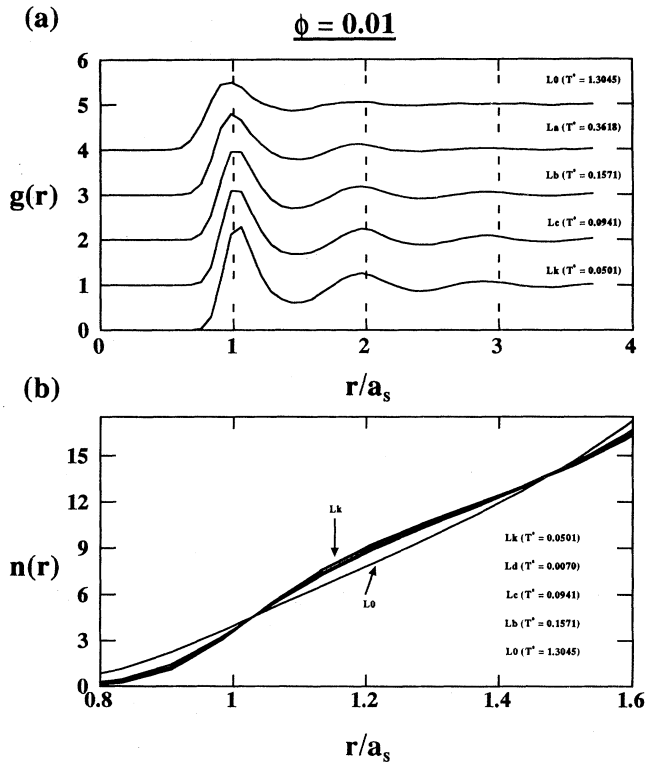


FIG. 5. (a) $g(r)$ vs $r/a_s$ for $\phi = 0.01$. (b) Number of neighbors $n(r)$ vs $r/a_s$ in the vicinity of the first peak of $g(r)$. For clarity, data for only a few runs (or $T^\star$), as marked in (a) and (b), are shown and curves for $g(r)$ are vertically shifted from each other by unity.

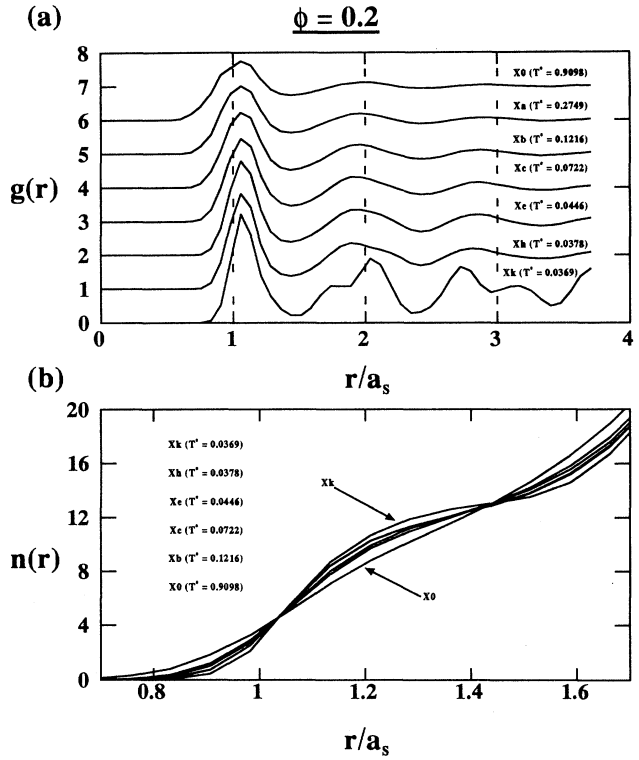


FIG. 6. Same as in Fig. 2, but for $\phi = 0.2$. Curves for the runs Xe and Xh in panel (b) overlap.

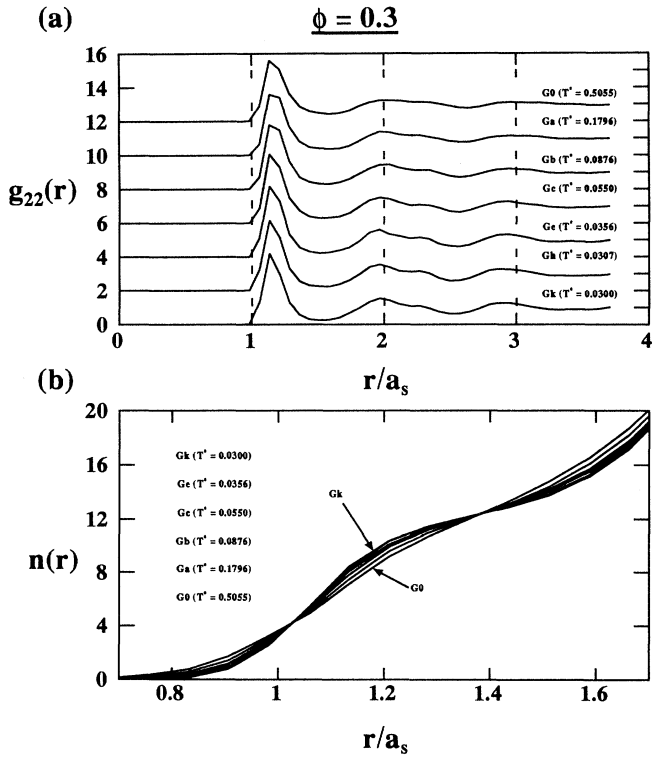


FIG. 7. (a) $g_{22}(r)$ vs $r/a_s$ for $\phi = 0.3$. The curves are vertically shifted from each other by $2a_s$. (b) $n(r)$ vs $r/a_s$ for the same value of $\phi$. The runs and the corresponding $T^*$ are marked.

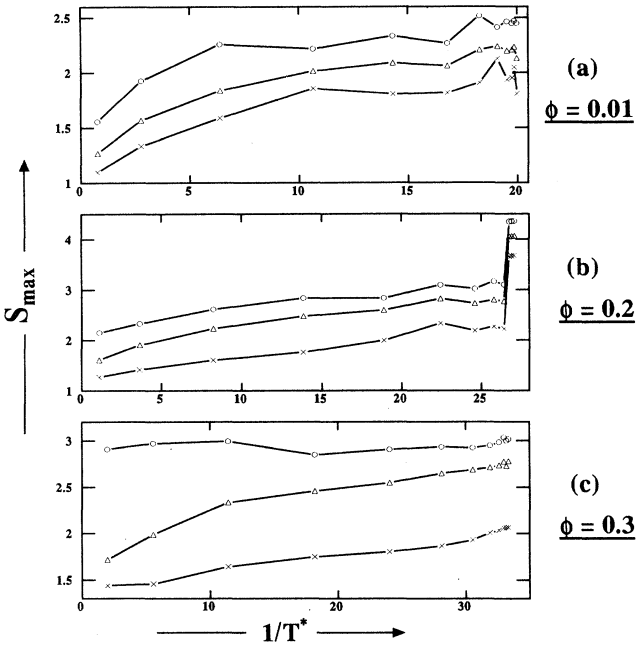


FIG. 8. Temperature dependence of the first-peak height $S_{\max}$ of the structure factors for (a) $\phi = 0.01$, (b) $\phi = 0.2$, and (c) $\phi = 0.3$. The data for the total, the lighter and the heavier sublattices are shown by triangles, circles, and crosses, respectively.

point [51] occurs at $r/a_s = 1.475 \pm 0.002$, corresponding to the first minimum following the first peak of $g(r)$. The value of $n(r)$ at this inflection point (which is taken to be the number of neighbors in the first coordination shell) is $13.7 \pm 0.1$. This suggests that the liquid has a bcc-like local order for which this value should have been 14.

For $\phi = 0.2$ (Fig. 6), the general nature of the development of PDF's and $S(q)$ in fluid phase (run X0 to run Xh) is similar to that for $\phi = 0.01$. The liquid to bcc crystal transition occurs over a few BD steps in the run Xi and then onward (i.e., for the final states of Xi, Xj, and Xk) the total and the partial PDF's show enhanced peaks at bcc peak positions [refer to Figs. 6(a), 2(b), 2(e), and 3(a)]. The PDF's [or the $S(q)$] of runs Xi, Xj, and Xk match perfectly well with each other, indicating an equilibrium situation. In Fig. 6(b) the value of $n(r)$ at the inflection point ($r/a_s = 1.474 \pm 0.003$) is $13.6 \pm 0.2$. This signifies bcc-like local order, supporting the Alexander-McTague prediction [52] that isotropic systems preferably crystallize into a bcc structure. This and the basic features of the total $g(r)$ for the liquid and the crystalline phases as above are in qualitative agreement with a previous detailed MD study of the monodisperse Yukawa system [51]. The $S_{\max}$ smoothly increases as the temperature is reduced and shows a jump at the liquid to the CT [Fig. 8(b)]. In particular, the value of $S_{\max}$ agrees with the Hansen-Verlet criterion [53] of approximately 2.8 over a small but finite range of temperatures near freezing.

The situation depicted in Fig. 7 for $\phi = 0.3$ shows

a completely different scenario for the PDF. As $T^\star$ decreases, the second peak splits into two and the third peak becomes more distinct. The sublattice PDF's show these features more clearly than the total PDF's and hence are shown here. Figure 8(c) clearly shows a smooth change of $S_{\max}$. A high value of $S_{\max}$ ($\sim$ 3) for the heavier sublattice at $T^\star \sim 0.5$ as compared to that for the lighter sublattice indicates that the heavier sublattice has already frozen. These characteristics are similar to the experimental results on complex glasses [42]. The smooth change over of the static quantities [e.g., the total and the partial PDF's, $S(q)$, $S_{\max}$, etc.] points towards the kinetic nature of the GT and is one of the basic predictions of the recent MCT [5]. In contrast to the above cases, the $n(r)$ in Fig. 7(b) shows that the value of $n(r) = 12.47 \pm 0.05$ at the inflection point ($r/a_s = 1.38 \pm 0.002$), indicating the local order to be fcc [38], supporting the similar inference drawn from Fig. 4.

### 3. *Wendt-Abraham parameter*

An empirical structural parameter $R_g = g_{\min}/g_{\max}$ has been used in previous computer simulations [38–40] to define the glass transition temperature $T_g$. The parameter $R_g$ shows a discontinuity in its slope as a function of $T$. A similar trend in $R_g$ versus the impurity concentration $n_i$ has been seen in Monte Carlo simulations of charge-polydisperse colloids [21,54]. In Fig. 9 we show our results for $R_g$ versus $n_i/(n_p\bar{Z})$. By fitting straight lines to the low $n_i$ and the high $n_i$ for $\phi = 0.3$ [panel (b)], we find that the value of $R_g$ at the intersection of the two lines is 0.1404, close to the value found in LJ systems [38,39,41] and charge-polydisperse colloids [21,54]. The value $(n_i)_g = 0.0339 n_p\bar{Z}$ provides the GT temperature $T_g^\star = 0.0312$. For the CT data in Fig. 9(a), $R_g$ shows a distinct jump at $(n_i)_g/(n_p\bar{Z}) = 5/512$ estimating the freezing temperature to be $T_f^\star = 0.0374$.

### 4. *Comparison of the run Xk with Xl and Xm*

A complete overlap of $g(r)$ and $g_{\alpha\beta}(r)$ for the runs Xk and Xl and the fact that the value of the internal energy $E$ for Xk is $118.67 \pm 0.04$, nearly the same as $118.45 \pm 0.04$ for compositionally disordered Xl, indicates that the final state Xk is a compositionally disordered bcc crystal. As stated earlier, we believe that given enough time and a larger system size, the final state might be a sublattice-ordered bcc structure, similar to the run Xm, for which $E$ is about 7% lower (equal to $110.74 \pm 0.02$). In order to check how good the bcc order is we have picked up four arbitrary particles in the simulation box and listed the distances and the types of their corresponding eight nearest neighbors. A comparison is made with the results of runs Xl and Xm both in their respective initial configurations and in the final state after simulating for $4 \times 10^5 \delta t$. For a perfect substitutional bcc lattice (initial configuration for run Xm), the immediate eight neighbors belong to the different species and they sit at the corners of a perfect cube with the concerned particle at the center of the cube. These particles, when simulated (the final state of run Xm), make movements (less than 5%) from their respective initial positions and seldom particles of the similar species become neighbors. In run Xl, the particles continuously rearrange themselves, irrespec-

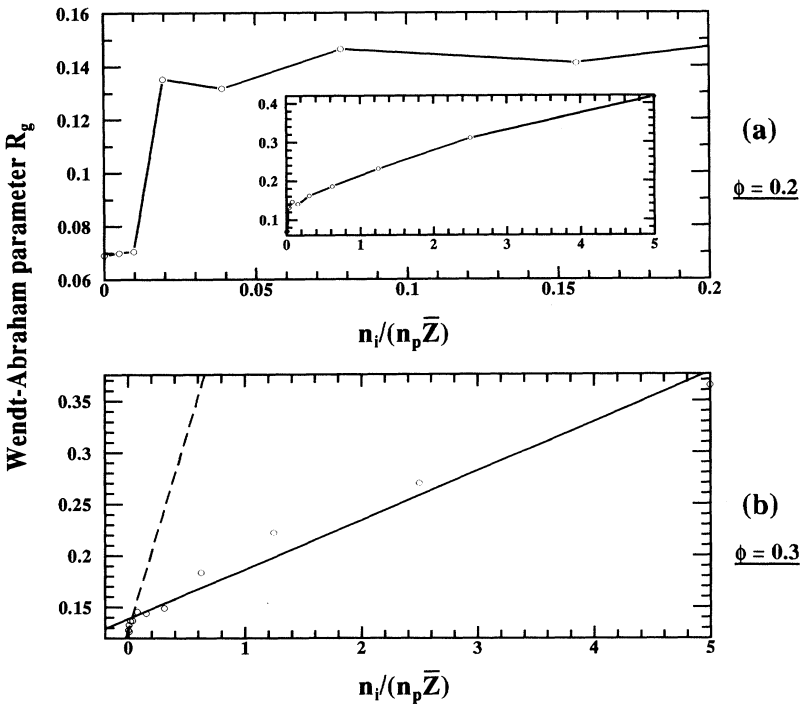


FIG. 9. $R_g$ vs $n_i/(n_p\bar{Z})$ for (a) $\phi = 0.2$ and (b) $\phi = 0.3$. The data in (a) are shown for $0 \le n_i/(n_p\bar{Z}) \le 0.2$, while those in the inset and in panel (b) are for $0 \le n_i/(n_p\bar{Z}) \le 5$. Straight lines fitted to the low-$n_i$ and the high-$n_i$ data in (b) are shown by dashed and continuous lines, respectively.

tive of their types, and this is in much closer comparison with the run Xk. This convincingly confirms that the final state Xk is a bcc crystal with an improper sublattice ordering.

### C. Mean-squared displacement

In order to quantify the dynamical evolution of the system, as it is cooled from an initial fluid phase, we have calculated the total mean-squared displacement defined by

$$\langle[\Delta\vec{r}(t)]^2\rangle_{t_0} = \left\langle \frac{1}{N}\sum_{i=1}^{N}[\vec{r}_i(t+t_0)-\vec{r}_i(t_0)]^2 \right\rangle_{t_0} \quad (9)$$

and also the partial MSD $\langle[\Delta\vec{r}_\alpha(t)]^2\rangle_{t_0}$ for both types of particles ($\alpha = 1$ or 2), defined similarly as in Eq. (9), where $\vec{r}_i(t)$ is the position of the particle $i$ at time $t$. The angular brackets in Eq. (9) indicate an averaging over a set of typically 50 initial conditions $\{t_0\}$ chosen at different times in the same run to improve the signal-to-noise ratio. The time dependence of the total MSD (the Einstein plots) are shown in Figs. 10 ($\phi = 0.2$) and 11 ($\phi = 0.3$) in log-log plots for various temperatures while cooling the system towards the $n_i = 0$ state. The sublattice MSD's carry information similar to that of the total MSD's and hence are not shown here. The power-law dependence of the MSD's can be expressed as $\langle[\Delta\vec{r}(t)]^2\rangle_{t_0} \propto t^m$, where the exponent $m = 1$ for Fickian diffusion and $m < 1$ for subdiffusion. The log-log plot is

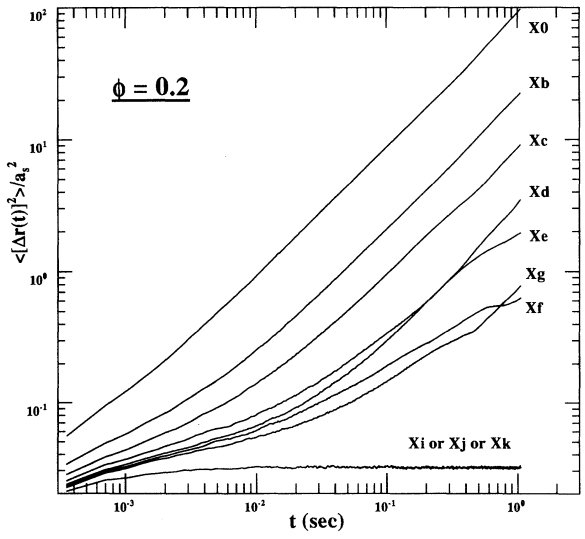


FIG. 10. The log-log plot of the temporal evolution of the total mean-squared displacements for the runs with $\phi = 0.2$ listed in Table I.

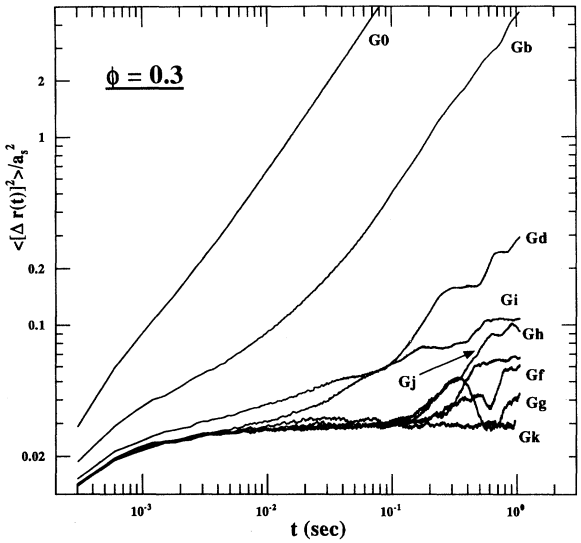


FIG. 11. Same as Fig. 10, but for $\phi = 0.3$.

a convenient way to present the data since MSD's with a power-law dependence should show up as a straight line with slope $m$ in this plot and hence the distinction between the diffusive and the subdiffusive regimes should be quite apparent.

At high temperatures the dynamics is considerably diffusive ($m = 1$ for all $t$) whereas they are localized or trapped ($m = 0$ for all $t$) in runs Xk and Gk at lowest $T^\star$. By contrast, the MSD for the final state Lk for $\phi = 0.01$ (not shown) still shows diffusive behavior ($m = 1$). These, along with the corresponding PDF's presented in Fig. 2, confirm the states Lk, Xk, and Gk to be liquid, crystalline, and glassy, respectively. At intermediate temperatures the general nature of the MSD follows three distinct stages. The initial stage can be associated with the "cage diffusion." This regime spans up to $t \sim 10^{-3}$ sec in the data for $\phi = 0.3$, but the choice of $\delta t$ does not allow us to see this regime for $\phi = 0.2$. Following this, there is an intermediate "subdiffusive" regime and the long-time diffusive behavior. Figures 10 and 11 clearly show that the linear temporal dependence of the MSD and hence approximating the long-time diffusion constant from the asymptotic slope of MSD's are valid for runs X0 to Xc for $\phi = 0.2$ and runs G0 to Gb for $\phi = 0.3$. As seen from Figs. 10 and 11, the long-time diffusion constant is lower than the short-time cage diffusion. The MSD's in other runs for both $\phi$'s have the following noteworthy features. The span of the subdiffusive regime increases successively as the temperature is lowered for both $\phi$'s and, as expected, it is more for the denser system ($\phi = 0.3$). Near the glass transition, this regime covers the entire simulation length and the asymptotic values of the diffusion constants are not reached. A clear difference between the nature of MSD's as a liquid is cooled towards a crystalline and a glassy state, as ap-

parent from curves Xd to Xk in Fig. 10 and curves Gc to Gk in Fig. 11, is that the MSD's in the latter show a "staircase" behavior that is completely absent in the former case. This supports the cage concept, indicating that in the supercooled or glassy regime, a particle repeatedly gets arrested in some kind of a cage structure formed by its neighbors and intermediately hops from one cage to another, giving rise to the observed staircase nature of the MSD. The fact that these are seen in the statistically averaged quantity MSD indicates that the hoppings must be taking place quite cooperatively. We note that since the MSD is quite small for these low temperature states, cooperative hops of the order of interparticle separation by a few particle will always show up in these plots. To confirm this conjecture, we have carried out a detailed study of the van Hove correlation functions and the individual particle displacements in the vicinity of the GT, which will be presented elsewhere [33]. We also note that a reduction in the long-time value of the MSD for the CT is sharp (curves Xh and Xi in Fig. 10) as compared to the slow kinetic nature of the GT.

## IV. SUMMARY AND CONCLUSIONS

In this paper we have presented the BD simulation results for a simple DLVO model of a binary mixture of polyballs with different radii and charges. The interest has been to look into the static and the dynamic aspects of this system in the liquid, crystal, and glassy states. By comparing different cooling methods, we infer the slow-quench method to be the most realistic and close to the method adopted in the laboratory experiments. The structural quantities studied are the total and the partial pair distribution functions $g(r)$ and their spatial Fourier transforms the static structure factors $S(q)$, the time averaged $g(\bar{r})$, and the Wendt-Abraham parameter $R_g = g_{\min}/g_{\max}$ and the dynamic quantity reported in this paper is the total mean-squared displacement. All these parameters show that by lowering the effective temperature (achieved by reducing the co-ion concentration $n_i$) at $\phi = 0.2$, liquid freezes into a body-centered-cubic crystal with imperfect sublattice ordering whereas at $\phi = 0.3$, a glassy state is reached. This result is in qualitative agreement with our DWS experiments [36] with binary mixtures.

The structural quantities and the mean-square displacements change abruptly at the crystal transition, expected of a first-order phase transition. On the contrary, slow and gradual changes of these quantities reveal the kinetic nature of the glass transition. The final state bcc lattice (run Xk) obtained by the slow cooling of a liquid for $\phi = 0.2$ has an imperfect sublattice ordering. Since a substitutional bcc lattice, with the same parameters as above (run Xm), has a lower potential energy per particle, we expect that the imperfect bcc lattice (run Xk) is metastable with a slightly higher energy. The change of slope of the Abraham-Wendt parameter estimates the freezing temperature $T_f^\star = 0.0374$ for $\phi = 0.2$ and the glass transition temperature $T_g^\star = 0.0312$ for $\phi = 0.3$. The value of $T_g^\star$ compares well with that obtained from analyzing the translational and bond-orientational correlation functions of the same system, presented in paper II [32]. The short-range order, beyond the principal minimum of the PDF, is shown to be bcc-like in the liquid, but is fcc-like in the glass. The structure is better revealed by the temperature averaged $g(\bar{r})$. With $g(\bar{r})$, the characteristic structural features in the PDF, namely, the short-range fcc order, the split second peak in the glass and the reversal of the relative subpeak intensities with interaction were discussed in the light of a recent paper by Clarke and Jónsson [49].

The mean-squared displacement changes with cooling from a normal liquid to a somewhat moderately cooled liquid, irrespective of the volume fraction. The temporal evolution of the MSD shows a deviation from the usual Fickian diffusion in the intermediate and long time for both $\phi$'s at low $n_i$. The temporal span of this subdiffusive regime increases with a decrease in the temperature as well as with increasing $\phi$. In the long-time regime, the MSD for supercooled liquid with $\phi = 0.3$ shows staircase behavior, indicating a strongly cooperative jump motion present in these states. This is a recent observation of the subdiffusive and staircase behavior for a system of Brownian particles. The subdiffusive behavior has been very recently calculated [55] and has been noted in the MD simulations of one-component and binary $r^{-12}$ soft-sphere systems [56,57], monodisperse Yukawa fluid [51,58,59] and LJ systems [60,61], and also for the nearest-neighbor-interacting lattice gas [62]. It has been suggested that the motion of a particle in the background of an inhomogeneous medium may lead to the subdiffusion. Approximating the long-time diffusion constant from the asymptotic slope of the MSD is strictly correct in the fluid phase, before the subdiffusive and staircase behaviors set in.

## ACKNOWLEDGMENTS

We thank the Indo-French Centre for the Promotion of Advanced Research (Project No. 607.1) for financial support. We made use of the computational resources of the Jawaharlal Nehru Centre for Advanced Scientific Research, India and the Supercomputer and Educational Research Center of the Indian Institute of Science, India. We thank Professor Jayant Banawar for useful discussions. S.S. acknowledges useful discussions with Siddhartha Shankar Ghosh and Jaydeb Chakrabarti at various stages of the work.

[1] B. J. Alder and T. E. Wainwright, J. Chem. Phys. **27**, 1208 (1957); W. W. Wood and J. D. Jacobson, *ibid.* **27**, 1207 (1957); W. G. Hoover and F. H. Ree, *ibid.* **47**, 4873 (1967).

[2] For reviews, see D. Frenkel and J. P. McTauge, Annu. Rev. Phys. Chem. **31**, 491 (1986); D. W. Oxtoby, Adv. Chem. Phys. **70**, 263 (1988).

[3] J. D. Bernal, Nature (London) **183**, 141 (1959); **185**, 68 (1960); Proc. R. Soc. London, Ser. A **280**, 299 (1964); J. D. Bernal and J. Mason, Nature (London) **188**, 910 (1960); G. D. Scott, *ibid.* **188**, 908 (1960); **194**, 956 (1962); **201**, 382 (1964); J. Chem. Phys. **40**, 611 (1964); M. H. Cohen and D. Turnbull, *ibid.* **31**, 1164 (1959); **34**, 120 (1961); **52**, 3038 (1970); Nature (London) **203**, 964 (1964); D. Turnbull, J. Phys. (Paris) Colloq. **35**, C4-1 (1974); M. Cohen and G. Grest, Phys. Rev. B **20**, 1077 (1979); G. Grest and M. H. Cohen, Adv. Chem. Phys. **48**, 455 (1981); D. Turnbull and M. Cohen, J. Chem. Phys. **34**, 120 (1961).

[4] For reviews, see C. A. Angell, J. H. R. Clarke, and L. V. Woodcock, Adv. Chem. Phys. **48**, 397 (1981); J. Jäckle, Rep. Prog. Phys. **49**, 171 (1986); Philos. Mag. B **56**, 113 (1987).

[5] For reviews on MCT, see W. Götze, in *Liquids, Freezing and the Glass Transition*, Proceedings of the Les Houches Summer School of Theoretical Physics, Session L1, edited by J. P. Hansen, D. Levesque, and J. Zinn-Justin (North-Holland, Amsterdam, 1991), p. 287; W. Götze and L. Sjögren, Rep. Prog. Phys. **55**, 241 (1992).

[6] F. Mezei, W. Knaak, and B. Farago, Phys. Rev. Lett. **58**, 571 (1978); **54**, 571 (1987); Phys. Scr. **T19**, 363 (1987); W. Knaak, F. Mezei, and B. Farago, Europhys. Lett. **7**, 529 (1988).

[7] L. Börjesson, M. Elmroth, and L. M. Torell, Chem. Phys. **149**, 209 (1990).

[8] F. Fujara and W. Petry, Europhys. Lett. **4**, 921 (1987); E. Bartsch, F. Fujara, M. Kiebel, H. Sillescu, and W. Petry, Ber. Bunsenges. Phys. Chem. **93**, 1252 (1989); W. Petry, E. Bartsch, F. Fujara, M. Kiebel, H. Sillescu, and B. Farago, Z. Phys. B **83**, 175 (1991).

[9] B. Frick, D. Ritcher, W. Petry, and U. Buchenau, Z. Phys. B **70**, 73 (1988); D. Ritcher, B. Frick, and B. Farago, Phys. Rev. Lett. **61**, 2465 (1988); B. Frick, D. Ritcher, and Cl. Ritter, Europhys. Lett. **9**, 557 (1989); B. Frick, B. Farago, and D. Ritcher, Phys. Rev. Lett. **64**, 2921 (1990).

[10] D. Doster, S. Cusack, and W. Petry, Phys. Rev. Lett. **65**, 1080 (1990).

[11] P. N. Pusey and W. van Megen, Nature **320**, 340 (1986); Phys. Rev. Lett. **69**, 2083 (1987).

[12] W. van Megen and P. N. Pusey, Phys. Rev. A **43**, 5429 (1991); W. van Megen, S. M. Underwood, and P. N. Pusey, Phys. Rev. Lett. **67**, 1586 (1991).

[13] P. N. Pusey and W. van Megen, Ber. Bunsenges. Phys. Chem. **94**, 225 (1990).

[14] For a review, see A. K. Sood, in *Solid State Physics*, edited by H. Ehrenreich and D. Turnbull (Academic, New York, 1991), Vol. 45, p. 1.

[15] K. Kremer, M. O. Robbins, and G. S. Grest, Phys. Rev. Lett. **57**, 2694 (1986).

[16] M. O. Robbins, K. Kremer, and G. S. Grest, J. Chem. Phys. **88**, 3286 (1988).

[17] R. O. Rosenberg and D. Thirumalai, Phys. Rev. A **36**, 5690 (1987).

[18] W. van Megen and I. Snook, Adv. Colloid. Interface Sci. **21**, 119 (1984).

[19] C. A. Castillo, R. Rajagopalan, and C. S. Hirtzel, Rev. Chem. Eng. **2**, 237 (1984).

[20] R. O. Rosenberg, D. Thirumalai, and R. D. Mountain, J. Phys. Condens. Matter **1**, 2109 (1989).

[21] B. V. R. Tata and A. K. Arora, J. Phys. Condens. Matter **4**, 7699 (1992).

[22] H. Löwen, J. P. Hansen, and J. N. Roux, Phys. Rev. A **44**, 1169 (1991).

[23] Y. Monovoukas and A. P. Gast, J. Colloid. Interface Sci. **128**, 533 (1989).

[24] E. B. Sirota, H. D. Ou-Yang, S. K. Sinha, P. M. Chaikin, J. D. Axe, and Y. Fujji, Phys. Rev. Lett. **62**, 1524 (1989).

[25] H. M. Lindsay and P. M. Chaikin, J. Chem. Phys. **76**, 3774 (1982).

[26] E. Dickinson, R. Perker, and M. Lal, Chem. Phys. Lett. **79**, 578 (1981); E. Dickinson and R. Perker, J. Phys. Lett. (Paris) **46**, L229 (1985).

[27] J. L. Barrat and J. P. Hansen, J. Phys. (Paris) **47**, 1547 (1986).

[28] P. N. Pusey, J. Phys. (Paris) **48**, 709 (1987).

[29] D. L. Ermak and Y. Yeh, Chem. Phys. Lett. **24**, 243 (1974); D. L. Ermak, J. Chem. Phys. **62**, 4189 (1975); **62**, 4197 (1975).

[30] D. L. Ermak and J. A. McCammon, J. Chem. Phys. **69**, 1352 (1978).

[31] K. Gaylor, I. Snook, and W. van Megen, J. Chem. Phys. **75**, 1682 (1980); J. Chem. Soc. Faraday Trans. II **76**, 1067 (1980); K. Gaylor, I. Snook, W. van Megen, and R. O. Watts, J. Phys. A **13**, 2513 (1980); W. van Megen and I. Snook, J. Chem. Phys. **78**, 931 (1983); **88**, 1185 (1988); G. Negele, M. Medina-Noyola, and R. Klein, Physica A **149**, 123 (1988).

[32] S. Sanyal and A. K. Sood, following paper, Phys. Rev. E **52**, 4168 (1995).

[33] S. Sanyal and A. K. Sood (unpublished).

[34] M. P. Allen and D. J. Tildesley, *Computer Simulation of Liquids* (Oxford University Press, London, 1987).

[35] M. J. Stevens, M. O. Robbins, and J. F. Belak, Phys. Rev. Lett. **66**, 3004 (1991).

[36] S. Sanyal and A. K. Sood, Pramana–J. Phys. **45**, 1 (1995).

[37] S. Sanyal, Ph.D. dissertation, Indian Institute of Science, 1994 (unpublished).

[38] F. F. Abraham, J. Chem. Phys. **72**, 359 (1980).

[39] H. R. Wendt and F. F. Abraham, Phys. Rev. Lett. **41**, 1244 (1978).

[40] H. J. Revenché, R. D. Mountain, and W. B. Streett, J. Chem. Phys. **61**, 1970 (1974).

[41] F. Yonezawa, in *Solid State Physics*, edited by E. Ehrenreich and D. Turnbull (Academic, New York, 1990), Vol. 45, p. 179.

[42] J. F. Sadoc and J. Dixmier, Mater. Sci. Eng. **23**, 187 (1976).

[43] B. Bernu, Y. Hiwatari, and J. P. Hansen, J. Phys. C **18**, L371 (1985); B. Bernu, J. P. Hansen, Y. Hiwatari, and G. Pastore, Phys. Rev. A **36**, 4891 (1987).

[44] G. S. Cargill III, in *Solid State Physics*, edited by E. Ehrenreich and D. Turnbull (Academic New York, 1975), Vol. 30, p. 227.

[45] G. Wahnström, Phys. Rev. A **44**, 3752 (1991).

[46] G. S. Cargill III and S. Kirkpatrick, in *Structure and Excitation of Amorphous Solids*, edited by G. Lucovsky

and F. L. Galeener, AIP Conf. Proc. No. 31 (American Institute of Physics, New York, 1976).
[47] M. Kimura and F. Yonezawa, in *Topological Disorder in Condense Matter*, edited by F. Yonezawa and T. Ninomiya (Springer-Verlag, Berlin, 1983), p. 80.
[48] J. L. Finney, Proc. R. Soc. London, Ser. A **319**, 479 (1970).
[49] A. Clarke and H. Jónsson, Phys. Rev. E **47**, 3975 (1993).
[50] J. L. Finney, Mater. Sci. Eng. **23**, 199 (1970).
[51] M. O. Robbins, K. Kremer, and G. S. Grest, J. Chem. Phys. **88**, 3286 (1988).
[52] S. Alexander and J. P. McTague, Phys. Rev. Lett. **41**, 702 (1978).
[53] J. P. Hansen and L. Verlet, Phys. Rev. **184**, 151 (1969).
[54] B. V. R. Tata and A. K. Arora, J. Phys. Condens. Matter **3**, 7983 (1991).
[55] A. V. Indrani and S. Ramaswamy, Phys. Rev. Lett. **73**, 360 (1994).
[56] Y. Hiwatari, B. Bernu and J. P. Hansen, in *Condensed Matter Theories*, edited by P. Vasishta, Rajiv K. Kalia, and R. F. Bishop (Plenum, New York, 1987), Vol. 2, p. 19.
[57] Y. Hiwatari, J. Phys. Soc. Jpn. **47**, 733 (1979); S. Kambayashi and Y. Hiwatari, *ibid.* **56**, 2788 (1987).
[58] K. Kremer, G. S. Grest, and M. O. Robbins, J. Phys. A **20**, L181 (1987).
[59] Micheal Wild and R. B. Pandey, Phys. Rev. E **47**, 3246 (1993).
[60] J. Ullo and S. Yip, Chem. Phys. **149**, 221 (1990).
[61] F. Ould-Kaddour and J.-L. Barrat, Phys. Rev. A **45**, 2308 (1992).
[62] P. Maass, J. Petersen, A. Bunde, W. Dietrich, and H. E. Roman, Phys. Rev. Lett. **66**, 52 (1991); P. Maass, A. Bunde, and M. D. Ingram, *ibid.* **68** 3064 (1992); R. B. Pandey, Physica A **191**, 438 (1992); **187**, 77 (1992).